Vibrational Spectroscopy of L-Valyl-Glycyl-Glycine, a Parallel-Chain β-Structure*

JAGDEESH BANDEKAR and S. KRIMM, *Biophysics Research Division and Department of Physics, University of Michigan, Ann Arbor, Michigan 48109*

Synopsis

Bands in the ir and Raman spectra of L-valyl-glycyl-glycine (VGG) and VGG-ND have been assigned on the basis of a normal mode analysis of the known parallel-chain β-structure of this tripeptide. Amide I, II, III, and V mode shifts are obtained by the interactions of dipole derivatives in symmetry coordinates, referred to as dipole derivative coupling. These derivatives, obtained from ab initio studies, are also used to calculate ir intensities of amide I, II, and V modes. The agreement between predicted and observed frequencies and intensities is very good, providing confidence in the application of our force fields to the calculation of the vibrational modes of the general parallel-chain β-sheet structure (following paper).

INTRODUCTION

Our extensive vibrational spectroscopic studies of peptides and polypeptides[1] have shown how normal mode analysis can be used to interpret ir and Raman spectra in terms of chain conformation. In addition to characterizing the standard α-helix, antiparallel-chain β-sheet, and β- and γ-turn secondary structures in this way, we have used such analyses to demonstrate the existence of the "extended-helix" conformation in polypeptides with charged side chains.[2] The force fields developed in these studies thus exhibit broad applicability to a variety of polypeptide conformations.

One of the structures not yet treated is the parallel-chain β-sheet. Although a common motif in proteins,[3] this structure has not as yet been identified in polypeptides (it has been claimed to be present in some oligopeptides,[4] but the spectral assignments were not rigorously founded). We have therefore computed the normal mode spectrum of the parallel-chain β-sheet, the results for which are presented in the following paper.[5]

In order to place these calculations in perspective, it seemed useful to do an analysis for a known parallel-chain β-structure. In the present paper, we present such a study for L-valyl-glycyl-glycine (VGG), a tripeptide known from single-crystal x-ray studies to form a parallel-chain β-structure.[6] Since the NH_3^+ and CO_2^- end groups are a significant part of the structure, and therefore of the spectra, we have refined the force constants for these groups in the VGG structure, starting with assignments and values from glycine[7] and triglycine (T. Sundius, J. Bandekar, and S. Krimm, to be published). In

*This is paper number 38 in a series on "Vibrational Analysis of Peptides, Polypeptides, and Proteins," of which paper number 37 is Ref. 27.

Biopolymers, Vol. 27, 885–908 (1988)

CCC 0006-3525/88/060885-24$04.00

addition, we have used our recently calculated ab initio dipole derivatives of the peptide group[8,9] to compute amide mode interaction splittings and ir intensities.

The results of these studies show that the ir and Raman bands of VGG and N-deuterated VGG (VGG-ND) can be interpreted completely and in excellent agreement with calculated frequencies. This strengthens our confidence in the analysis of the general parallel-chain β-sheet structure.[5]

EXPERIMENTAL

Samples of VGG were a gift from Prof. E. Subramanian of the Department of Crystallography and Biophysics of the University of Madras, India. Single crystals grown from this material were used in the x-ray studies.[6] The N-deuterated material was obtained by dissolving ~ 5 mg of VGG in ~ 5 mL D_2O for about 36 h and then freeze drying; this procedure was repeated three times. (Just drying under vacuum proved to be unsuccessful: the initial moisture present in the vacuum chamber was apparently sufficient to cause a reexchange of ND_3^+ to NH_3^+.)

Infrared spectra were obtained in KBr disks or, for the far ir, pressed films of the powder, at room and liquid N_2 (LN_2) temperatures. The spectrometer was a Bomem DA3 FTIR instrument, operated at a resolution of 2 cm^{-1}. Raman spectra were obtained from powders in a capillary tube, using a Spex 1403 spectrometer and 5145 Å excitation. The laser power was 400 mW, and a spectral bandwidth of ~ 1 cm^{-1} was used. Infrared spectra of VGG and VGG-ND are given in Fig. 1, and Raman spectra are presented in Fig. 2.

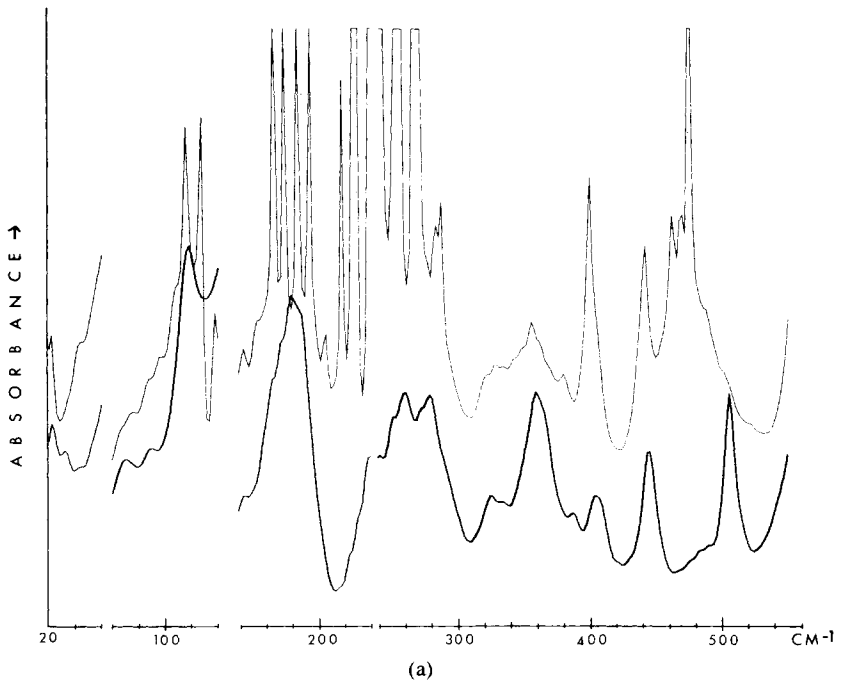

(a)

Fig. 1. Infrared spectra of VGG (heavy line) and VGG-ND (light line). (Some bands in the 160–280-cm^{-1} region of the ND compound are totally absorbing because of the thickness of the sample.)

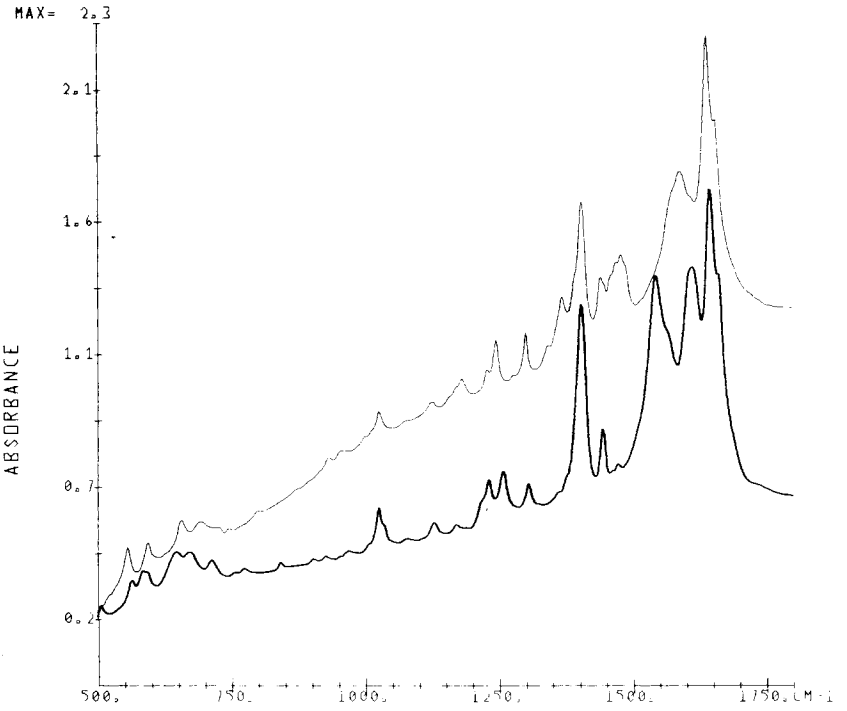

(b)

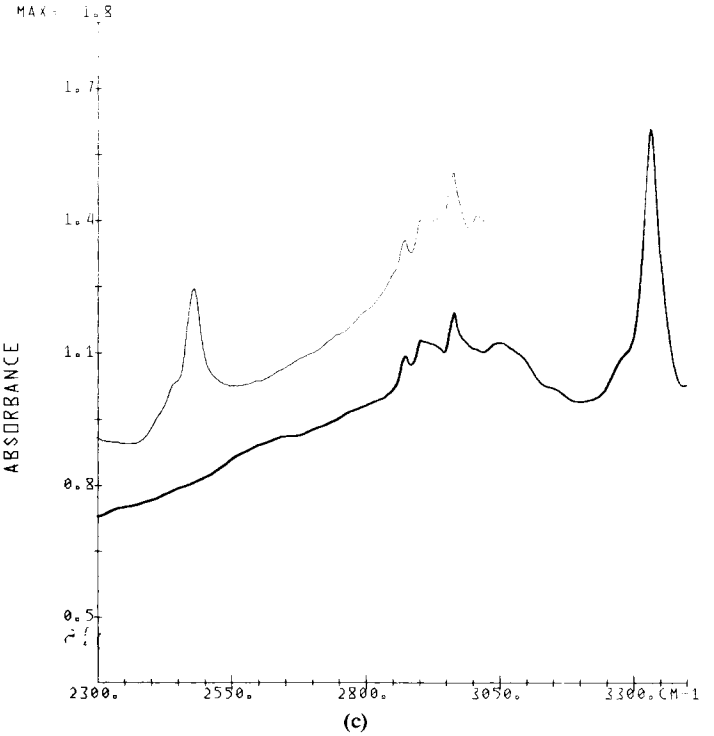

(c)

Fig. 1. (*Continued from the previous page.*)

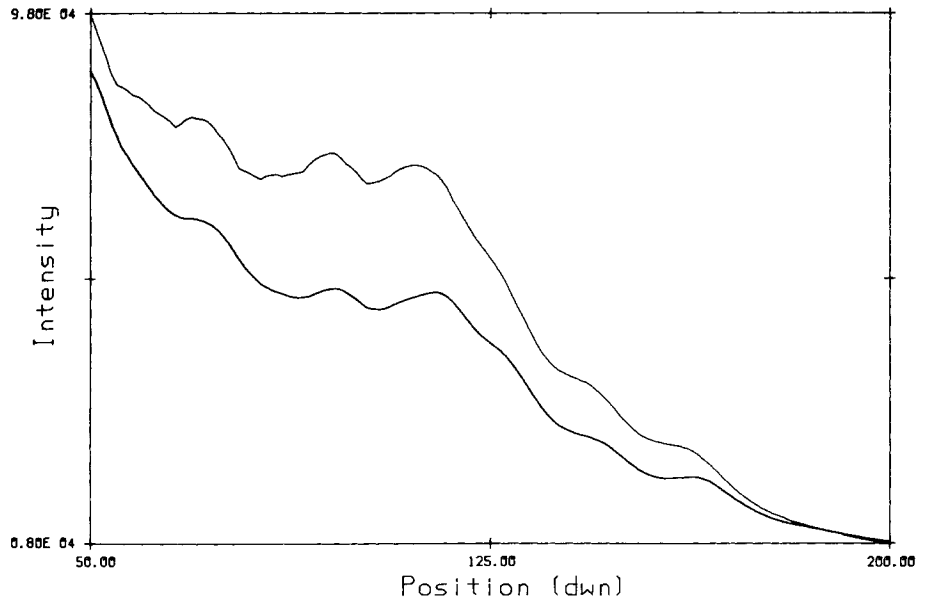

(a)

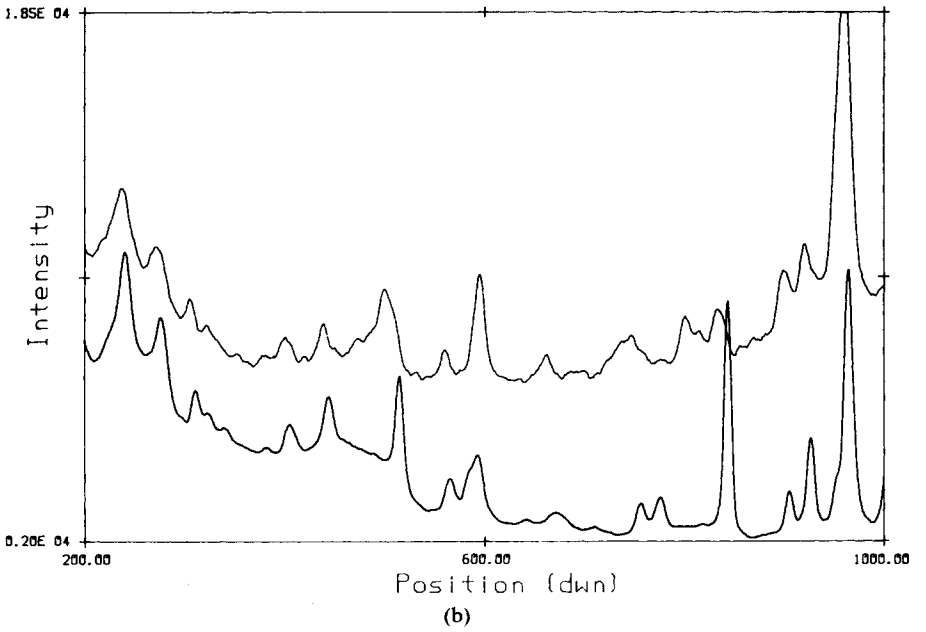

(b)

Fig. 2. Raman spectra of VGG (heavy line) and VGG-ND (light line).

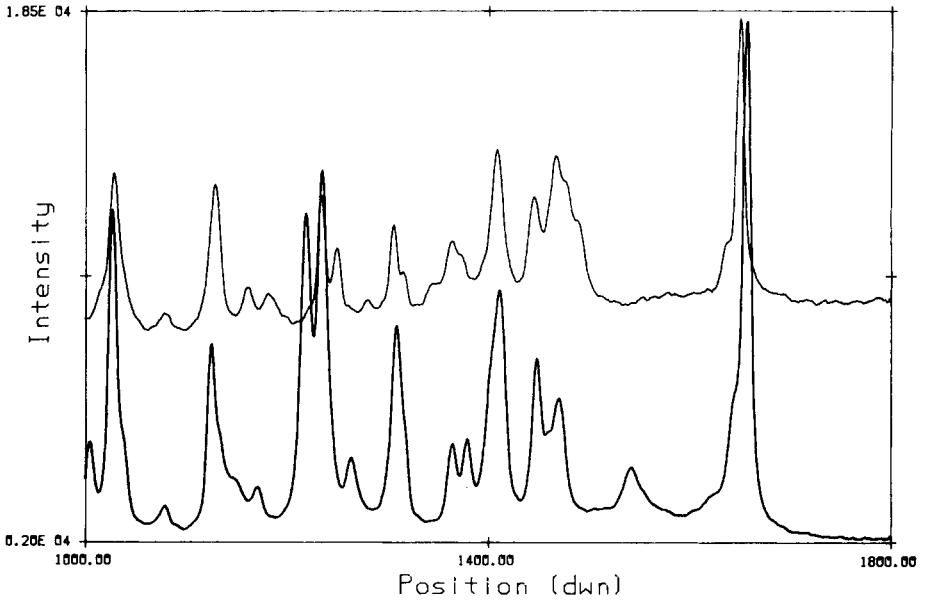

(c)

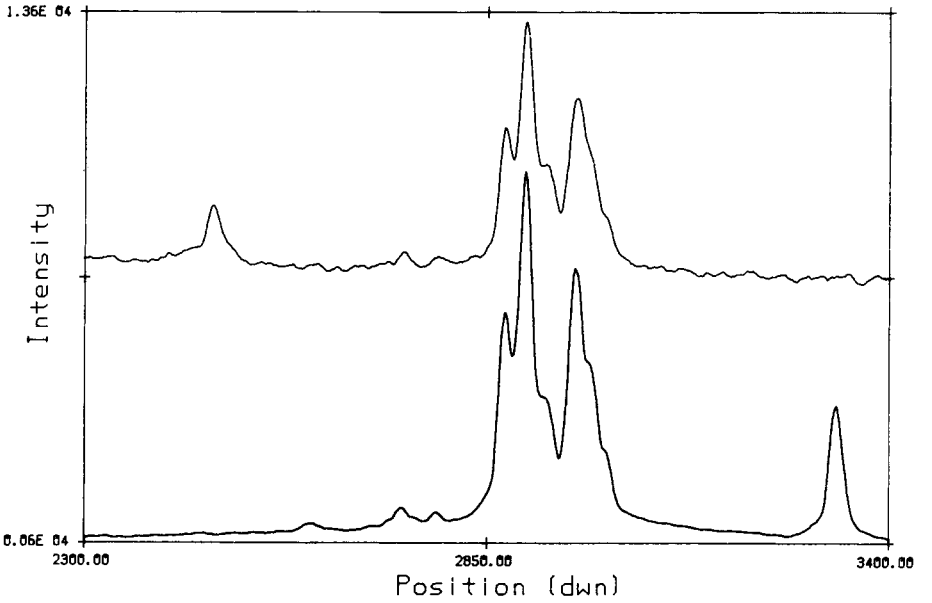

(d)

Fig. 2. (*Continued from the previous page.*)

NORMAL MODE CALCULATIONS

The unit cell of VGG is monoclinic, space group $C2$, with $a = 24.058$ Å, $b = 4.801$ Å, $c = 10.623$ Å, $\beta = 110.02°$, and $Z = 4$.[6] The parallel-chain β-structure is in the ab plane, with hydrogen bonds directed along the b axis [see Fig. 3(a)]. Adjacent sheets perpendicular to the ab plane are oppositely directed, and are related by a twofold axis across which the NH_3^+ and CO_2^- end groups of four molecules are hydrogen bonded [see Fig. 3(b)].

The molecule appears to be the most extended observed so far, with the peptide chain repeat $d(C_1^\alpha\text{-}C_3^\alpha) = 7.23$ Å [see Fig. 3(c)]. The backbone torsion angles are $\psi_1 = 123.1°$, $\omega_1 = -179.4°$, $\phi_2 = -155.1°$, $\psi_2 = 154.7°$, $\omega_2 = 170.7°$, $\phi_3 = -146.6°$, and $\psi_3 = 180.0°$. The peptide hydrogen bonds are rather weak, with $d(N_2 \ldots O_1') = 3.052$ Å, $\theta(N_2\text{-}H_2 \ldots O_1') = 149.5°$, $d(H_2 \ldots O_1') = 2.23$ Å and $d(N_3 \ldots O_2') = 3.049$ Å, $\theta(N_3\text{-}H_3 \ldots O_2') = 152.4°$, $d(H_3 \ldots O_2') = 2.19$ Å. On the other hand, the hydrogen bonds between the end groups are reasonably strong: $d(N_1 \ldots O_3'') = 2.887$ Å, $\theta(N_1\text{-}H_1 \ldots O_3'') = 155.7°$, $d(H_1 \ldots O_3'') = 1.99$ Å; $d(N_1 \ldots O_3'') = 2.805$ Å, $\theta(N_1\text{-}H_2 \ldots O_3'') = 144.1°$, $d(H_2 \ldots O_3'') = 1.93$ Å; and $d(N_1 \ldots O_3') = 2.758$ Å, $\theta(N_1\text{-}H_3 \ldots O_3') = 171.5°$, $d(H_3 \ldots O_3') = 1.86$ Å.

In order to transfer our polypeptide force constants, it was necessary to use standard bond lengths and angles, including planar peptide groups.[1] We therefore regenerated the crystal structure with such geometry but with the ϕ, ψ dihedral angles as originally given.[6] For the valyl side chain, the following parameters were used: $d(C_1^\alpha\text{-}C^\beta) = 1.54$ Å, $d(C^\beta\text{-}C^\gamma) = 1.54$ Å, $d(C^\gamma\text{-}H) = 1.09$ Å; all angles about C^β and C^γ were tetrahedral; the dihedral angles were $\tau(N_1\text{-}C_1^\alpha\text{-}C^\beta\text{-}H^\beta) = 120.0°$, $\tau(N_1\text{-}C_1^\alpha\text{-}C^\beta\text{-}C_1^\gamma) = 0°$, $\tau(N_1\text{-}C_1^\alpha\text{-}C^\beta\text{-}C_2^\gamma) = -120.0°$, $\tau(C_1^\alpha\text{-}C^\beta\text{-}C^\gamma\text{-}H_1) = -120.0°$, $\tau(C_1^\alpha\text{-}C^\beta\text{-}C^\gamma\text{-}H_2) = 0°$, $\tau(C_1^\alpha\text{-}C^\beta\text{-}C^\gamma\text{-}H_3) = 120.0°$. For the end groups we used $d(N_1\text{-}H^+) = 1.037$ Å, $d(C\text{-}O^-) = 1.249$ Å, angles about N_1 tetrahedral, $\theta(C_3^\alpha CO^-) = 112.23°$, $\tau(H_1\text{-}N_1\text{-}C_1^\alpha\text{-}C_1) = 120.0°$, $\tau(H_2\text{-}N_1\text{-}C_1^\alpha\text{-}C_1) = 0°$, $\tau(H_3\text{-}N_1\text{-}C_1^\alpha\text{-}C_1) = -120.0°$, $\tau(N_3\text{-}C_3^\alpha\text{-}C\text{-}O') = -4.0°$, $\tau(N_3\text{-}C_3^\alpha\text{-}C\text{-}O'') = -180.0°$.

The internal (R) and local symmetry (S) coordinates of the peptide chain have been defined as in our earlier work.[1] Such coordinates for the valyl side chain are given in Table I. The CO_2^- wagging coordinate of the trigonal planar $C_3^\alpha CO_2^-$ group is defined as an out-of-plane bend by $\Delta\omega = \Delta\alpha \sin(OCO)$, where $\Delta\alpha$ is the displacement of the $C_3^\alpha C$ bond from the OCO plane.

Although there are four molecules in the monoclinic unit cell, the primitive unit cell contains two molecules.[10] The $3n - 3 = 195$ normal modes (n = number of atoms) divide into 98 A species and 97 B species, both of which are ir and Raman active.

The force constants for the peptide chain were transferred from the force fields for polyglycine I[11] and β-poly(L-alanine).[12,13] The initial force constants for the valyl side chain were taken from the work of Snyder and Schachtschneider on branched paraffins.[14] While slight refinement of these force constants led to satisfactory frequencies below 1800 cm^{-1}, the computed CH_3 stretching modes were found to be rather low. Changing the stretching force constants associated with the CH_3 groups to those for β-poly(L-alanine)[12,13] led to surprisingly good agreement with observation. The final force constants are given in Table II. As noted above, for the NH_3^+ and CO_2^- end groups, we started with force constants for glycine and tri-

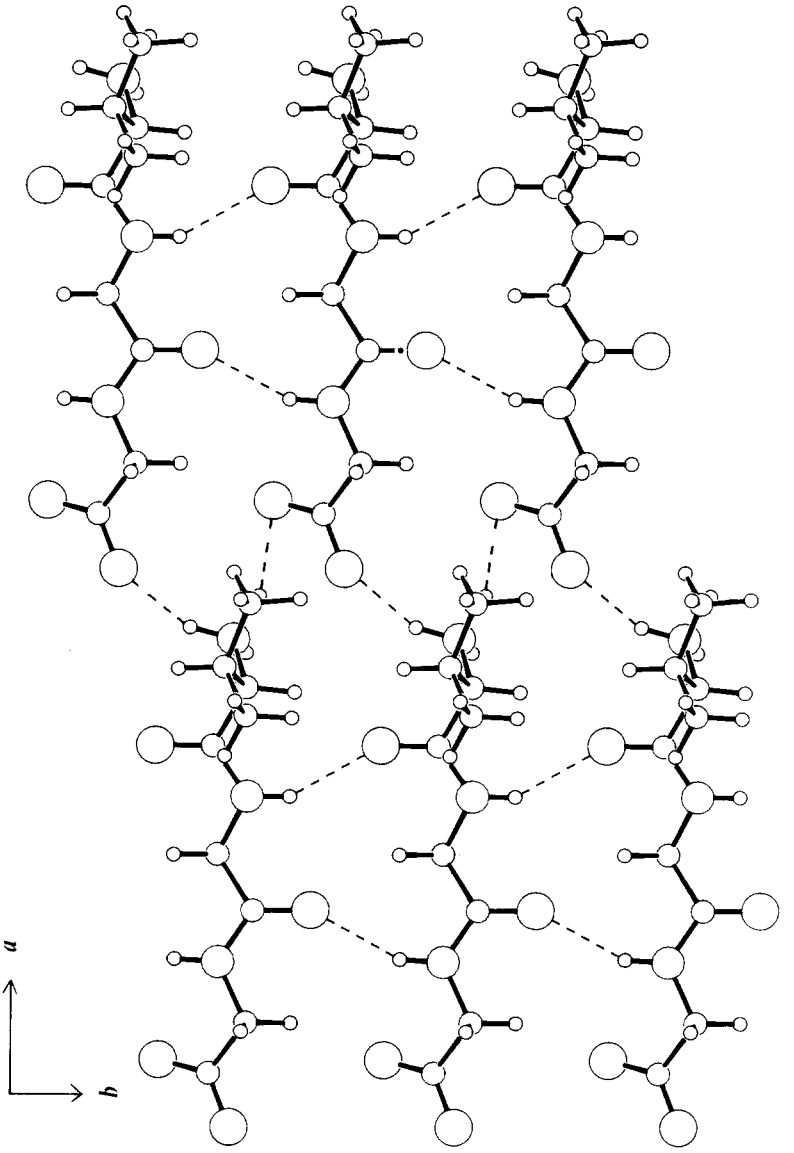

(a)

Fig. 3. Crystal structure of VGG.[6]: (a) *a b* section, (b) *a c* projection, and (c) atom numbering in one molecule.

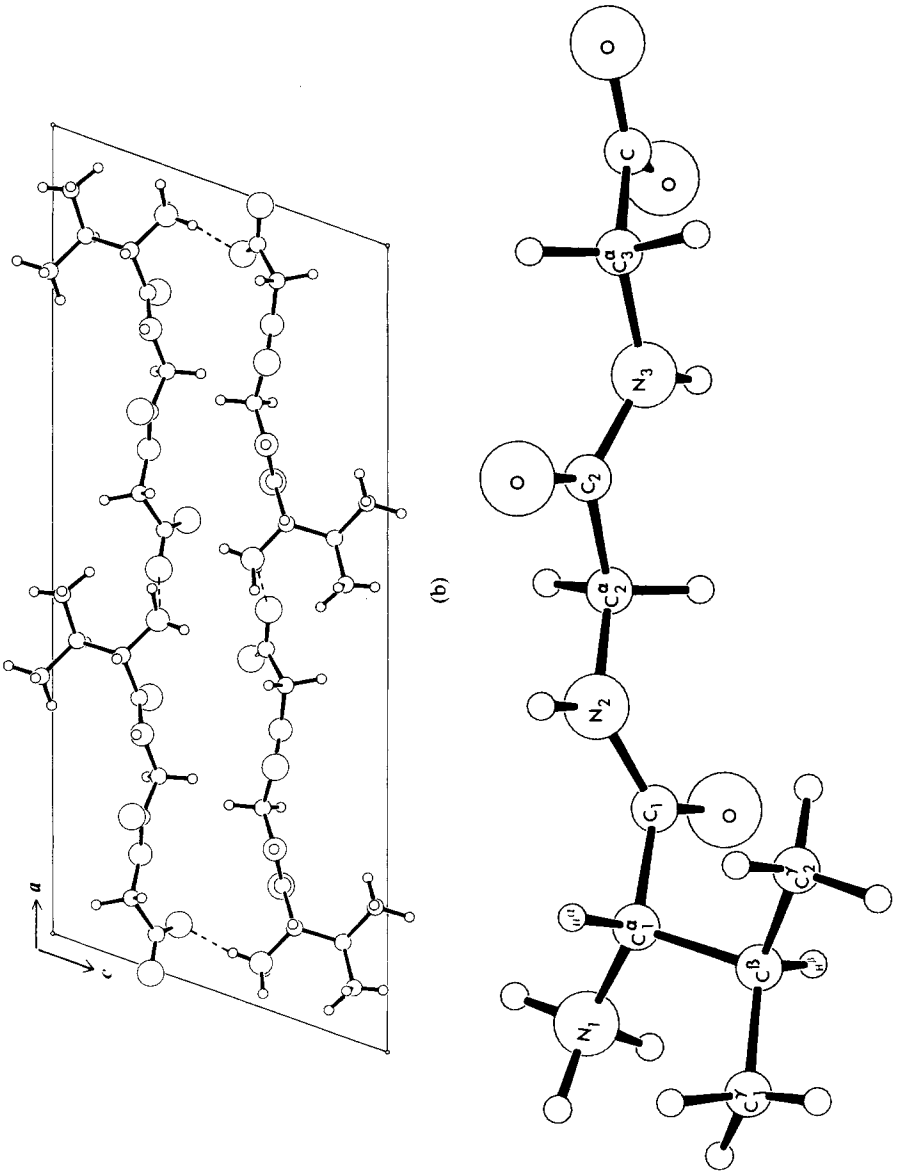

Fig. 3. (*Continued from the previous page.*)

TABLE I
Coordinates for the Valyl Side Chain

Internal Coordinates[a]	
$R_1 = \Delta r(C_1^\alpha H^\alpha)$	$R_{17} = \Delta\theta(C^\beta C_1^\gamma H)$
$R_2 = \Delta r(C_1^\alpha C^\beta)$	$R_{18} = \Delta\theta(HC_2^\gamma H)$
$R_3 = \Delta r(C^\beta H^\beta)$	$R_{19} = \Delta\theta(HC_2^\gamma H)$
$R_4 = \Delta r(C^\beta C_1^\gamma)$	$R_{20} = \Delta\theta(HC_2^\gamma H)$
$R_5 = \Delta r(C_1^\gamma H)$	$R_{21} = \Delta\theta(C^\beta C_2^\gamma H)$
$R_6 = \Delta r(C_1^\gamma H)$	$R_{22} = \Delta\theta(C^\beta C_2^\gamma H)$
$R_7 = \Delta r(C_1^\gamma H)$	$R_{23} = \Delta\theta(C^\beta C_2^\gamma H)$
$R_8 = \Delta r(C^\beta C_2^\gamma)$	$R_{24} = \Delta\theta(C_1^\alpha C^\beta C_1^\gamma)$
$R_9 = \Delta r(C_2^\gamma H)$	$R_{25} = \Delta\theta(C_1^\alpha C^\beta C_2^\gamma)$
$R_{10} = \Delta r(C_2^\gamma H)$	$R_{26} = \Delta\theta(C_1^\gamma C^\beta C_2^\gamma)$
$R_{11} = \Delta r(C_2^\gamma H)$	$R_{27} = \Delta\theta(C_1^\alpha C^\beta H^\beta)$
$R_{12} = \Delta\theta(HC_1^\gamma H)$	$R_{28} = \Delta\theta(C_1^\alpha C^\beta C_1^\gamma)$
$R_{13} = \Delta\theta(HC_1^\gamma H)$	$R_{29} = \Delta\theta(H^\beta C^\beta C_1^\gamma)$
$R_{14} = \Delta\theta(HC_1^\gamma H)$	$R_{30} = \Delta\tau(C_1^\alpha C^\beta)$
$R_{15} = \Delta\theta(C^\beta C_1^\gamma H)$	$R_{31} = \Delta\tau(C^\beta C_1^\gamma)$
$R_{16} = \Delta\theta(C^\beta C_1^\gamma H)$	$R_{32} = \Delta\tau(C^\beta C_2^\gamma)$
Symmetry Coordinates[b]	
$S_1 = R_1$	$C_1^\alpha H^\alpha$ s
$S_2 = R_2$	$C_1^\alpha C^\beta$ s
$S_3 = R_3$	$C^\beta H^\beta$ s
$S_4 = R_4$	$C^\beta C_1^\gamma$ s
$S_5 = R_5 + R_6 + R_7$	$C_1^\gamma H_3$ ss
$S_6 = 2R_7 - R_5 - R_6$	$C_1^\gamma H_3$ as1
$S_7 = R_5 - R_6$	$C_1^\gamma H_3$ as2
$S_8 = R_8$	$C^\beta C_2^\gamma$ s
$S_9 = R_9 + R_{10} + R_{11}$	$C_2^\gamma H_3$ ss
$S_{10} = 2R_{11} - R_{10} - R_9$	$C_2^\gamma H_3$ as1
$S_{11} = R_9 - R_{10}$	$C_2^\gamma H_3$ as2
$S_{12} = R_{12} + R_{13} + R_{14} - R_{15} - R_{16} - R_{17}$	$C_1^\gamma H_3$ sb
$S_{13} = 2R_{12} - R_{13} - R_{14}$	$C_1^\gamma H_3$ ab1
$S_{14} = R_{13} - R_{14}$	$C_1^\gamma H_3$ ab2
$S_{15} = 2R_{15} - R_{16} - R_{17}$	$C_1^\gamma H_3$ r1
$S_{16} = R_{16} - R_{17}$	$C_1^\gamma H_3$ r2
$S_{17} = R_{18} + R_{19} + R_{20} + R_{21} + R_{22} + R_{23}$	$C_2^\gamma H_3$ sb
$S_{18} = 2R_{18} - R_{19} - R_{20}$	$C_2^\gamma H_3$ ab1
$S_{19} = R_{19} - R_{20}$	$C_2^\gamma H_3$ ab2
$S_{20} = 2R_{21} - R_{22} - R_{23}$	$C_2^\gamma H_3$ r1
$S_{21} = R_{22} - R_{23}$	$C_2^\gamma H_3$ r2
$S_{22} = R_{24} + R_{25} + R_{26} - R_{27} - R_{28} - R_{29}$	C^β d
$S_{23} = 2R_{24} - R_{25} - R_{26}$	C^γ b1
$S_{24} = R_{25} - R_{26}$	C^γ b2
$S_{25} = 2R_{27} - R_{28} - R_{29}$	H^β b1
$S_{26} = R_{28} - R_{29}$	H^β b2
$S_{27} = R_{30}$	$C_1^\alpha C^\beta$ t
$S_{28} = R_{31}$	$C^\beta C_1^\gamma$ t
$S_{29} = R_{32}$	$C^\beta C_2^\gamma$ t

[a] Δr, Bond stretch; $\Delta\theta$, angle bend; $\Delta\tau$, torsion.

[b] s, Stretch; ss, symmetric stretch; as, antisymmetric stretch; b, bend; sb, symmetric bend; ab, antisymmetric bend; d, deformation; r, rock, t, torsion.

TABLE II
Force Constants for Valyl Side Chain and for End Groups

	Force Constant[a]	Value[b]	Force Constant[a]	Value[b]
$CH(CH_3)_2$	$C^\alpha H^\alpha$	4.4628	$C^\alpha C^\beta, C^\alpha C^\beta H^\beta$	0.261
	$C^\alpha C^\beta$	4.980	$C^\alpha C^\beta, C^\alpha C^\beta C^\gamma$	0.351
	$C^\beta H^\beta$	4.590	$C^\beta C^\gamma, C^\alpha C^\beta C^\gamma$	0.351
	$C^\beta C^\gamma$	4.394	$C^\beta C^\gamma, C^\gamma C^\beta C^\gamma$	0.351
	$C^\gamma H$	4.800	$C^\beta C^\gamma, C^\beta C^\gamma H$	0.328
	$C^\alpha C^\beta H^\beta$	0.555	$C^\beta C^\gamma, HC^\gamma H$	0.047
	$C^\alpha C^\beta C^\gamma$	1.230	$NC^\alpha C^\beta, C^\alpha C^\beta C^\gamma$	0.072
	$H^\beta C^\beta C^\gamma$	0.667	$H^\alpha C^\alpha C^\beta, C^\alpha C^\beta H^\beta$	0.050
	$C^\beta C^\gamma H$	0.700	$C^\alpha C^\beta C^\gamma, C^\alpha C^\beta H^\beta$	−0.124
	$C^\gamma C^\beta C^\gamma$	0.901	$C^\alpha C^\beta C^\gamma, C^\alpha C^\beta C^\gamma$	0.043
	$HC^\gamma H$	0.524	$(C^\alpha C^\beta C^\gamma, C^\beta C^\gamma H)_T$	0.072
	$C^\beta C^\gamma$ t	0.072	$(C^\alpha C^\beta C^\gamma, C^\beta C^\gamma H)_G$	−0.058
	$C^\alpha C^\beta, C^\beta C^\gamma$	0.064	$C^\alpha C^\beta C^\gamma, C^\gamma C^\beta C^\gamma$	0.043
	$C^\beta C^\gamma, C^\beta C^\gamma$	0.064	$(H^\beta C^\beta C^\gamma, C^\beta C^\gamma H)_T$	0.040
	$C^\gamma H, C^\gamma H$	0.071	$(H^\beta C^\beta C^\gamma, C^\beta C^\gamma H)_G$	−0.024
	$C^\alpha C^\beta, CC^\alpha C^\beta$	0.367	$C^\beta C^\gamma H, C^\beta C^\gamma H$	−0.045
NH_3^+	NH	5.163	NC^α, HNH	−0.150
	NC^α	4.823	$NC^\alpha, NC^\alpha C$	0.600
	HNH	0.549	$NC^\alpha, NC^\alpha H^\alpha$	0.627
			$C^\alpha C, NC^\alpha C$	0.300
	HNC^α	0.829	$C^\alpha C^\beta, NC^\alpha H^\alpha$	0.079
	$NC^\alpha H^\alpha$	0.765	$C^\alpha C^\beta, NC^\alpha C^\beta$	0.317
	$NC^\alpha C$	0.819		
	NC^α t	0.250	HNH, HNH	−0.015
	N-H t	0.0005	HNC^α, HNC^α	−0.040
	NH, NH	0.022	$NC^\alpha C, NC^\alpha C^\beta$	0.150
	$NC^\alpha, C^\alpha C$	0.300		
	NC^α, HNC^α	0.294	$NC^\alpha C, C^\beta C^\alpha C$	−0.141
CO_2^-	CO	9.500	CO, OCO	−0.135
	OCO	2.100	CO, $C^\alpha CO$	0.700
	OCC^α	1.109	$CO_1, C^\alpha CO_2$	−0.509
	CO...H	0.010	$C^\alpha C$, OCO	−0.652
	$C^\alpha C$ t	0.155	$C^\alpha C, C^\alpha CO$	0.300
	C-O t	0.001	$C^\alpha CO, C^\alpha CO$	−0.100
	CO_2 w	0.577	CO_2 w, $CC^\alpha H^1$	−0.093
	CO, CO	1.400	CO_2 w, $CC^\alpha H^2$	0.093
	CO, $C^\alpha C$	0.9584		

[a]AB: AB bond stretch; ABC: ABC angle bend; X, Y: XY interaction; t, torsion; w, wag; T, *trans*; G, *gauche*.

[b]Units: mdyn/Å for stretch and stretch, stretch force constants; mdyn for stretch, bend constants; mdyn Å for all others.

glycine, and modified these slightly to give optimum agreement for VGG. It is not surprising that such refinement is necessary, since the detailed environments of the end groups in VGG differ from those in the above structures. The force constants used for NH_3^+ and CO_2^- are also given in Table II. The end-group hydrogen-bond force constants correspond to the structural parameters of the original structure.[6]

In previous studies,[1,15,16] we computed the electrostatic coupling between similar amide vibrations by interacting dipole derivatives with respect to a normal coordinate, $\partial\mu/\partial Q_\alpha$, where the values of these derivatives were obtained by parametrizing observed splittings in the amide modes of β-poly(L-alanine). We referred to this as transition dipole coupling (TDC). Since the eigenvectors of these amide modes can vary between molecules, it is more reliable to obtain the interaction by directly coupling dipole derivatives with respect to the symmetry coordinates, viz., $\partial\mu/\partial S$, which we refer to as dipole derivative coupling (DDC). The values of the $\partial\mu/\partial S$ that we used were taken from our ab initio studies of the peptide group.[9] The intensities are proportional to $|\partial\mu/\partial Q_\alpha|^2$, where $(\partial\mu/\partial Q_\alpha) = \Sigma_i \mathbf{L}_{i\alpha}(\partial\mu/\partial S_i)$, with $\mathbf{L}$ the eigenvector matrix defined by $S = \mathbf{L}Q$.

RESULTS AND DISCUSSION

NH_3^+ and CO_2^- Modes

Since modes associated with the end groups are a significant part of the spectra, it is important to have reliable assignments for them so that the peptide-chain modes can be identified with confidence. We discuss the end-group modes first, comparing in Table III the assignments of these modes in VGG with those in some amino acids.[7,17-23] A complete description of the modes in VGG is given in Table IV, and of those in VGG-ND in Table V.

The unperturbed NH_3^+ antisymmetric stretch (as) and symmetric stretch (ss) modes are predicted at 3122 and 3115 and at 3034 cm^{-1}, respectively (see Table IV). The NH stretch (s) modes also occur in this general region, and are perturbed by Fermi resonance with combinations of amide II modes.[24] Similar perturbations may occur for the NH_3^+ s modes, and we have therefore not attempted at this time to assign these bands in detail, beyond noting that N-deuteration shows that such modes should be assigned to the complex of bands above 3030 cm^{-1}. The ND stretch region exhibits prominent bands at 2484S (ir), 2477MW (R), 2447VW (ir), 2444VW (R), 2417VW (R), 2330VW (R), and 2290MW (ir) cm^{-1}.

The NH_3^+ antisymmetric bend (ab) modes are clearly assigned to the strong and broad ir band centered at $\sim$ 1611 cm^{-1}, since this band disappears on N-deuteration. In the LN_2 temperature spectrum, components are clearly seen at 1616 and 1606 cm^{-1}; their 10 cm^{-1} splitting is significantly less than the predicted 23 cm^{-1} splitting, but no intergroup coupling was taken into account in the calculation. The ND_3^+ ab mode is predicted to dominate modes at 1162 and 1134 cm^{-1}, and a new Raman band is observed at 1161 cm^{-1}, and to contribute to the shift of the H^α bend 1 (b1) mode at 1168 cm^{-1} to a similar mode at 1188 cm^{-1}, which seems to account for the shift of the 1171 cm^{-1} band to $\sim$ 1185 cm^{-1}.

The NH_3^+ symmetric bend (sb) mode is calculated at 1517 cm^{-1}, and is observed in the 1498–1546 cm^{-1} range in amino acids (cf. Table III). It is probably assignable to a shoulder at $\sim$ 1510 cm^{-1} in the ir spectrum, which is clearly seen as a well-defined, very weak band at LN_2 temperature that disappears on N-deuteration. The ND_3^+ sb mode is predicted at 1098 cm^{-1}; it is possible that a new shoulder at $\sim$ 1084 cm^{-1} in the Raman is assignable to

TABLE III
Assignments of NH_3^+ and CO_2^- Modes in VGG and in Some Amino Acids

Mode	VGG	α-Gly		L-Ala					L-Ser
		7[a]	17	18	19	20	21	22	23
NH_3^+ ab	1616	~ 1610	*1669*[b]	*1647*		*1650*	*1645*	*1648*	1648
	1606	~ 1610	*1642*		1615	*1622*	*1625*		
			1610						
NH_3^+ sb	~ 1510	1520	1523	*1546*	1505	*1502*	*1498*	*1498*	1498
		1507	*1513*						
NH_3^+ r	(*1309*, 1307)[c]	1313							
	(*1264*, 1259)								
	1219, 1217			*1236*	1235	*1239*	*1220*	*1238*	1238
	(*1135*)	1130	*1139*	*1112*		*1146*	*1145*	*1143*	1143
		1110	1130						
NH_3^+ t	*515*, 506	520		*484*	481	*480*	*477*	*477*	477
CO_2^- as	1589[d]	~ 1587	1594	*1595*	1590	*1598*	*1607*	*1596*	1596
	1572[d]		*1570*						
CO_2^- ss	*1411*	1411	1415	1416	1414				1409
	1404		*1410*	*1409*		*1410*	*1410*	*1409*	
CO_2^- b	*776*, 774	697	698	*771*		*653*	*640*	*653*	653
	(*756*, 757)		*695*						
CO_2^- w	*593*, 592	607	608	*653*	769	*774*	*775*	*772*	772
	(*585*, 584)		*603*						
CO_2^- r	585, 584	501	503	*532*	642	*532*	*527*	*531*	531
	(*405*, 405)		*495*						

[a] From Ref. 7, etc.
[b] Italicized numbers refer to Raman bands, others to ir bands.
[c] Parentheses indicate small contribution to potential energy distribution (PED).
[d] Seen in spectra of Val-Gly-Gly-ND.

TABLE IV
Observed and Calculated Frequencies (in cm^{-1}) of VGG

Observed[a]		Calculated		
Raman	IR	A	B	Potential Energy Distribution[b]
3328M	3335S	3280	3280	N_2H s(98)
	3317 sh[d]	3278	3278	N_1H s(98)
3289VW	3285VW	3122	3122	H_3 as1(91)
	3160VW	3115	3115	H_3 as2(92)
	3076W	3034	3034	H_3 ss(97)
	3040M[d]			
3012 sh	3010VW[d]	3014	3014	$C_3^{\alpha}H_2$ as(100)
2992 sh				
	2975 sh[d]	2984	2984	$C_1^{\gamma}H_3$ as1(54) $C_2^{\gamma}H_3$ as2(32) $C_2^{\gamma}H_3$ as1(11)
2972S	2968M	2983	2983	$C_1^{\gamma}H_3$ as2(71) $C_2^{\gamma}H_3$ as2(16) $C_2^{\gamma}H_3$ as1(13)
	2961 sh[d]	2983	2983	$C_2^{\gamma}H_3$ as1(45) $C_1^{\gamma}H_3$ as2(26) $C_2^{\gamma}H_3$ as2(17)
		2982	2982	$C_1^{\gamma}H_3$ as1(45) $C_2^{\gamma}H_3$ as2(35) $C_2^{\gamma}H_3$ as1(19)
	2945VW[d]	2929	2929	$C_2^{\gamma}H_3$ ss(51) $C_1^{\gamma}H_3$ ss(50)
		2929	2929	$C_1^{\gamma}H_3$ ss(51) $C_2^{\gamma}H_3$ ss(50)
2930VW	2930VW[d]	2926	2926	$C_3^{\alpha}H_2$ ss(99)
	2918 sh[d]	2918	2918	$C_2^{\alpha}H_2$ as(99)
2902VS	2903M	2904	2904	$C^{\beta}H^{\beta}$ s(97)
2876W	2875W			Overtone
	2870 sh[d]	2866	2866	$C^{\alpha}H^{\alpha}$ s(98)
2850 sh	2850 sh	2851	2851	$C_2^{\alpha}H_2$ ss(99)
	1663W		1661[c]	C_1O s(68) C_1N s(22)
1657VS			1654[c]	C_2O s(76) C_2N s(15) $C_2^{\alpha}CN$ d(11)
1643W	1645VS	1645[c]		C_1O s(68) C_1N s(22)
		1643[c]		C_2O s(76) C_2N s(15) $C_2^{\alpha}CN$ d(11)
	1616S[d]	1632	1632	H_3 ab2(71) H_3 r1(13)
	1606S[d]	1609	1609	H_3 ab1(78) H_3 r2(11)
		1595[c]		N_2H ib(22) N_3H ib(20) C_2N s(11) $C_2^{\alpha}C$ s(11)
	(~ 1580[e])	1584	1584	O_2 as(104)
	1568VW		1564[c]	N_2H ib(22) N_3H ib(20) C_2N s(11) $C_2^{\alpha}C$ s(11)
1541MW	1543S		1541[c]	N_2H ib(24) N_3H ib(21) C_2N s(10) C_1N s(10)
		1531[c]		N_2H ib(24) N_3H ib(21) C_2N s(11) C_1N s(10)
	~ 1510 sh[d]	1517	1517	H_3 sb(79)
1470MW	1473W	1469	1469	C_1^{γ} ab1(40) H^{β} b2(18) C_2^{γ} ab1(14)
1459VW	1462VW	1462	1462	C_2^{γ} ab2(48) C_1^{γ} ab2(18)
		1455	1455	C_2^{γ} ab1(35) C_1^{γ} ab2(26) C_2^{γ} ab2(23)
		1454	1454	$C_2^{\alpha}H_2$ b(25) $C_3^{\alpha}H_2$ b(24) C_2^{γ} ab1(13)
1448M	1445M	1453	1453	C_1^{γ} ab2(40) C_2^{γ} ab1(21) C_1^{γ} ab1(11)
		1442	1442	$C_3^{\alpha}H_2$ b(48) $C_2^{\alpha}H_2$ b(38)
		1423	1423	H^{β} b2(35) C_1^{γ} ab1(18)
		1416	1416	$C_2^{\alpha}H_2$ b(19) $C_2^{\alpha}H_2$ w(19)
1411MS				
1403 sh	1404S	1400	1400	O_2 ss(53) O_2 b(27) $C_3^{\alpha}C$ s(16) $C_3^{\alpha}H_2$ b(13)
1379MW	1384 sh	1388[c]	1389[c]	$C_3^{\alpha}H_2$ w(24) H^{α} b2(14) $C_3^{\alpha}C$ s(10) N_2H ib(7)
		1366	1366	C_1^{γ} sb(54) C_2^{γ} sb(49)
1364MW	1362VW	1363	1363	C_2^{γ} sb(54) C_1^{γ} sb(48)
		1350	1350	$C_2^{\alpha}H_2$ w(30) $C_3^{\alpha}H_2$ w(28)
1309M	1307M	1316	1316	$C_1^{\alpha}C^{\beta}$ s(27) H^{α} b2(26) H_3 r1(12) H_3 sb(8) H_3 r2(7)
1264MW		1267[c]	1267[c]	H^{β} b1(33) N_2H ib(8) H_3 r1(8) H_3 r2(7)
	1259M	1260[c]	1260[c]	$C_3^{\alpha}H_2$ w(11) N_3H ib(11) H^{β} b1(10) H_3 r1(7)
		1251	1251	$C_2^{\alpha}H_2$ tw(38) $C_2^{\alpha}H_2$ w(15)
		1242	1242	$C_3^{\alpha}H_2$ tw(67) $C_2^{\alpha}H_2$ tw(19)
1235VS	1233M	1238[c]	1238[c]	$C_2^{\alpha}H_2$ tw(35) $C_3^{\alpha}H_2$ tw(13) N_3H ib(9) N_2H ib(8)
1219S	1217 sh	1208	1208	H_3 r2(47) H_3 r1(14) H^{α} b2(10) H_3 ab2(8)

TABLE IV

(Continued from the previous page)

Observed[a]		Calculated		
Raman	IR	A	B	Potential Energy Distribution[b]
1171W	1171W	1168	1168	H^{α} b1(30) C_2^{γ} r2(14) H_3 r2(7)
1150W				
1135 sh		1136	1136	NC_3^{α} s(22) NC_2^{α} s(21) H_3 r1(13)
1125M	1129MW	1127	1127	C_2^{γ} r1(25) C_1^{γ} r1(19) H^{β} b1(13)
		1101	1101	H^{α} b1(30) NC_3^{α} s(17) H_3 r1(10)
1079W	1078W	1073	1073	H^{β} b2(16) NC_3^{α} s(14) NC_1^{α} s(14) NC_2^{α} s(13) C_1^{γ} r2(12)
		1055	1055	NC_2^{α} s(16) H^{α} b1(15) C_1^{γ} r2(11) H^{β} b2(10)
1037 sh	1036VW	1033	1033	C_2^{γ} r2(44) C_1^{γ} r1(35) C_1^{γ} r2(10)
1027VS	1026M	1013	1013	NC_1^{α} s(69)
1004MW	1007VW	998	998	C_2^{γ} r1(33) $C^{\beta}C_1^{\gamma}$ s(21) $C^{\beta}C_2^{\gamma}$ s(13) NC_1^{α} s(12)
		994	994	$C_2^{\alpha}H_2$ r(42)
		983	983	C_1^{γ} r2(15) $C_1^{\alpha}C^{\beta}$ s(12)
965S	969W	972	972	$C_2^{\alpha}H_2$ r(20)
951 sh	954VW[d]	951	951	$C_3^{\alpha}H_2$ r(33) $C_3^{\alpha}C$ s(29) O_2 ss(12) O_2 b(12)
927MW	926W	936	935	$C_3^{\alpha}H_2$ r(46)
906W	904W	895	895	$C_1^{\alpha}C$ s(18) $C_2^{\alpha}H_2$ r(13) C_1N s(10)
844S	843W	835	835	$C^{\beta}C_1^{\gamma}$ s(32) $C^{\beta}C_2^{\gamma}$ s(28) $C_1^{\alpha}C^{\beta}$ s(10)
776W	774W	777	777	O_2 b(29) O_2 ss(10)
756W	757VW	750	751	C_1O ib(16) O_2 b(14) $C_1^{\alpha}C$ s(10)
709VW	714MW	698[c]	698[c]	C_2N t(63) N_3H ob(24) C_1N t(22) N_2H ob(8)
671W	675M	677[c]	677[c]	C_1N t(61) C_2N t(18) N_2H ob(17) N_3H ob(9)
	670VW[c]	662[c]	661[c]	C_1O ob(32) $C_1^{\alpha}CN$ d(10) N_2H ob(10)
641W	647M	654[c]	654[c]	C_1O ob(29) C_2O ib(20) N_2H ob(7)
593M	592MW	595	595	O_2 w(78)
585 sh	584MW	586	587	O_2 r(24) $C_2^{\alpha}CN$ d(18) O_2 w(17)
565W	564W	566[c]	566[c]	C_2O ob(65) N_3H ob(7)
515S		523	521	NC_1^{α} t(24) O_2 r(13) $H_3 \ldots O$ b(5)
	506 W	499	498	NC_1^{α} t(23) C^{γ} b1(10) $H_3 \ldots O$ b(6)
444M	445W	444	445	C^{β} d(51)
405MW	405W	417	419	C^{γ} b2(24) C^{β} d(14) O_2 r(12)
382W	388VW	394	394	C^{γ} b2(40) C^{β} b1(12) C^{γ} b1(10)
	360W			$2 \times 188 = 376$
340W	334VW			$2 \times 180 = 360$
325W	326VW	327	327	C_2O ib(14) $NC_2^{\alpha}C$ d(13) C^{β} b1(11) N_3H ob(5)
311MW		298		$NC_1^{\alpha}C$ d(22) $C_1^{\alpha}CN$ d(14) C^{γ} b1(12) C^{β} b1(11) $H_3 \ldots O$ s(14)
	297 sh		295	$NC_1^{\alpha}C$ d(18) C^{γ} b1(14) C_1O ib(12) C^{β} b1(11) $H_3 \ldots O$ s(7)
	280W	271		$NC_3^{\alpha}C$ d(17) C^{β} b1(13) N_3H ob(5)
277M			267	C^{β} b1(29) C^{γ} b1(23)
	260W	263		C^{β} b1(23) C^{γ} b1(21)
			260	$NC_3^{\alpha}C$ d(20) O_2 r(16)
240S	247W	249	249	C_2O ib(14) CNC_2^{α} d(13) CNC_3^{α} d(13) N_3H ob(12)
223 sh		226	225	CNC_3^{α} d(19) CNC_2^{α} d(18) $H_3 \ldots O$ s(5)
		217	216	C^{β} b2(37) N_2H ob(12) C^{γ} b2(11) $H_3 \ldots O$ s(6)
	188M	198	198	$C^{\beta}C_1^{\gamma}$ t(88)
	180M	197	197	$C^{\beta}C_2^{\gamma}$ t(84)
164VW	166 sh	163	159	$H_3 \ldots O$ s(25) $N_2H \ldots O$ s(6)
146VW	144VW	140	140	$NC_1^{\alpha}C$ d(18) C^{β} b2(18) $C_1^{\alpha}CN$ d(12) C_1O ob(11)
115W	116W	116		$N_3H \ldots O$ s(14) $H_3 \ldots O$ s(12)
109VW			109	$H_3 \ldots O$ s(10) $N_2H \ldots O$ s(10) $N_3H \ldots O$ s(10)
97W			102	$H_3 \ldots O$ s(58) N_2H ob(8)
		93		$C_3^{\alpha}C$ t(26) N_2H ob(10) NC_2^{α} t(10) $H_3 \ldots O$ s(7) $N_2H \ldots O$ s(6) N_3H ob(5)
	89W		86	$H_3 \ldots O$ s(19) $C_3^{\alpha}C$ t(15) NC_2^{α} t(11) $N_2H \ldots O$ s(7) N_2H ob(6) N_3H ob (6)
		83		$N_2H \ldots O$ s(14) $C_1^{\alpha}C^{\beta}$ t(11) $H_3 \ldots O$ s(9)

TABLE IV

(Continued from the previous page)

Observed[a]		Calculated		
Raman	IR	A	B	Potential Energy Distribution[b]
72W	70W		78	$C_3^{\alpha}C$ t(16) $C_1^{\alpha}C^{\beta}$ t(10) $H_3 \ldots O$ s(7) $N_2H \ldots O$ s(5) N_3H ob(5) N_2H ob(5)
		70		NC_3^{α} t(22) N_2H ob(13) $C_1^{\alpha}C^{\beta}$ t(12) N_3H ob(11)
			66	NC_3^{α} t(19) N_3H ob(18) $NC_3^{\alpha}C$ d(15) N_3H t(7) $N_3H \ldots O$ b(6) N_2H ob(5)
		61		N_3H ob(20) $NC_3^{\alpha}C$ d(18) $C_1^{\alpha}C^{\beta}$ t(10) $H_3 \ldots O$ b(9)
	54 sh		55	$C_1^{\alpha}C^{\beta}$ t(57) N_3H ob(7) $H_3 \ldots O$ s(6)
		50		$C_1^{\alpha}C^{\beta}$ t(49) $H_3 \ldots O$ s(5)
37 sh	38VW	38		$H_3 \ldots O$ b(17) NC_1^{α} t(14) $H_3 \ldots O$ s(15) $H_3 \ldots O$ t(14)
			38	$C_1^{\alpha}C^{\beta}$ t(19) $H_3 \ldots O$ t(13) NC_3^{α} t(11) N_2H ob(6) $H_3 \ldots O$ b(6)
			36	$H_3 \ldots O$ t(15) $H_3 \ldots O$ b(8) $H_3 \ldots O$ s(8) $N_2H \ldots O$ s(6) N_2H ob(5)
31VW	29VW	33		NC_3^{α} t(18) N_3H t(14) $H_3 \ldots O$ t(12) $N_3H \ldots O$ b(6)
			32	$H_3 \ldots O$ b(14) $C_1^{\alpha}C$ t(11) N_3H t(9) $H_3 \ldots O$ s(8) N_2H t(6)
		30		$H_3 \ldots O$ s(26) $NC_2^{\alpha}C$ d(12) $C_1^{\alpha}C^{\beta}$ t(10) N_2H ob(8)
			23	NC_3^{α} t(17) $H_3 \ldots O$ b(15) $C_2^{\alpha}C$ t(14) NC_1^{α} t(9)
		17		$C_1^{\alpha}C$ t(19) $H_3 \ldots O$ b(14) N_2H t(8) $N_3H \ldots O$ s(6) N_2H ob(5)
			15	$C_1^{\alpha}C$ t(24) N_2H ob(12) NC_2^{α} t(10) $N_3H \ldots O$ s(8) $H_3 \ldots O$ t(6) $H_3 \ldots O$ b(5)
		14		$H_3 \ldots O$ b(14) N_2H ob(12) $H_3 \ldots O$ s(11)
		8		$O_2 \ldots H$ b(24) $H_3 \ldots O$ t(23) CO^- t(10)

[a] S, strong; M, medium; W, weak; V, very; sh, shoulder.

[b] s, Stretch; ss, symmetric stretch; as, antisymmetric stretch; b, bend; sb, symmetric bend; ab, antisymmetric bend; ib, in-plane bend; ob, out-of-plane bend; d, deformation; w, wag; tw, twist; r, rock; H_3, NH_3^+; O_2, CO_2^-. Only contributions of 10 or greater are included, except for NH and NH_3^+, for which contributions of 5 or greater are included. In some cases, the value is an average of the PEDs for the A and B species. For the NH_3^+ group, $H_3 \ldots O$ s and $H_3 \ldots O$ b refer to the combined values of the three N-H bonds.

[c] Includes DDC interactions.

[d] Clearly visible in liquid N_2 temperature spectra.

[e] Inferred from presence in spectra of Val-Gly-Gly-ND.

TABLE V

Observed and Calculated Frequencies (in cm^{-1}) of VGG-ND

Observed[a]		Calculated		
Raman	IR	A	B	Potential Energy Distribution[b]
	1657W		1657[c]	C_1O s(70) C_1N s(22)
1650VS			1650[c]	C_2O s(75) C_2N s(15) $C_2^{\alpha}CN$ d(10)
1636W	1640VS	1641[c]		C_1O s(70) C_1N s(22)
		1639[c]		C_2O s(75) C_2N s(15) $C_2^{\alpha}CN$ d(10)
	1589M, 1572W[d]	1582	1582	O_2 as(109)
1491VW	1491W[d]	1490	1490	$C_2^{\alpha}C$ s(29) C_2N s(20) $C_2^{\alpha}H_2$ w(16) $C_2^{\alpha}H_2$ b(13) C_2O ib(12) N_3D ib(7)
1478VW	1480M	1481	1481	$C_1^{\alpha}C$ s(24) C_1N s(14) C_1O s(12) $C_1^{\alpha}CN$ d(12) H^{α} b2(10) N_2D ib(6)
1467S	1471VW[d]	1469	1469	C_1^{γ} ab1(33) H^{β} b2(19) C_2^{γ} ab1(14)
	1461VW	1459	1459	C_2^{γ} ab2(57)
	1449 sh	1455	1455	C_2^{γ} ab1(43) C_1^{γ} ab2(28) C_2^{γ} ab2(13)

TABLE V

(*Continued from the previous page*)

Observed[a]		Calculated		
Raman	IR	A	B	Potential Energy Distribution[b]
		1453	1453	C_1^{γ} ab2(45) C_2^{γ} ab1(27) C_1^{γ} ab1(14)
1445M	1442W	1450	1450	$C_3^{\alpha}H_2$ b(68)
		1431	1431	$C_2^{\alpha}H_2$ b(70) $C_3^{\alpha}H_2$ b(10)
		1422	1422	H^{β} b2(41) C_1^{γ} ab1(25)
1409S				
	1407S	1399	1400	O_2 ss(56) O_2 b(28) $C_3^{\alpha}C$ s(18) $C_3^{\alpha}H_2$ b(15)
	1395W[d]			
		1368	1367	C_1^{γ} sb(30) $C_3^{\alpha}H_2$ w(22) H^{α} b2(13)
1373W	1371W	1366	1366	$C_3^{\alpha}H_2$ w(37) C_1^{γ} sb(32) C_2^{γ} sb(19)
		1364	1364	C_2^{γ} sb(73)
1364MW		1361	1362	C_1^{γ} sb(36) H^{α} b2(24)
1315VW				
1344W		1345	1345	$C_2^{\alpha}H_2$ w(53) C_2N s(11)
1306M	1305M	1310	1310	$C_1^{\alpha}C^{\beta}$ s(31) H^{β} b1(27) H^{α} b2(21)
1280W	1282VW	1277	1277	$C_2^{\alpha}H_2$ tw(76) $C_3^{\alpha}H_2$ tw(13) $C_1^{\alpha}C^{\beta}$ s(10)
1250MW	1250M	1246	1246	$C_3^{\alpha}H_2$ tw(82) $C_2^{\alpha}H_2$ tw(13)
1235MS	1234W	1229	1223	H^{β} b1(40) $C_1^{\alpha}C^{\beta}$ s(12)
1182W	1187MW	1188	1188	H^{α} b1(30) D_3 ab1(12) D_3 sb(9)
1161W	1159VW	1162	1162	D_3 ab2(71) D_3 ab1(8) D_3 r1(5)
		1134	1134	D_3 ab1(62) D_3 ab2(8) D_3 r2(6)
		1129	1129	NC_3^{α} s(29) NC_2^{α} s(19)
1129MS	1127MW	1121	1121	C_2^{γ} r1(22) C_1^{γ} r1(16) NC_3^{α} s(13)
1084 sh		1098	1098	D_3 sb(76)
1078W	1079W	1073	1073	H^{β} b2(19) C_1^{γ} r2(18) NC_1^{α} s(14) $C^{\beta}C_2^{\gamma}$ s(11) D_3 sb(8)
1054VW		1055	1055	NC_2^{α} s(21) NC_3^{α} s(14) H^{α} b1(11) C_1^{γ} r2(11)
1040 sh	1039 sh[d]	1040	1040	N_2D ib(20) $C_2^{\alpha}H_2$ r(13) NC_3^{α} s(12)
		1034	1034	C_2^{γ} r2(27) N_3D ib(18) C_1^{γ} r1(12)
		1033	1033	C_2^{γ} r2(24) C_1^{γ} r1(18) N_3D ib(15)
1029S	1028MW	1017	1017	NC_1^{α} s(20) $C_1^{\alpha}C^{\beta}$ s(14) C_2^{γ} r2(14) C_2^{γ} r1(12) D_3 r1(9)
1014 sh	1015VW	1003	1003	NC_1^{α} s(23) C_2^{γ} r1(23) $C^{\beta}C_1^{\gamma}$ s(11) C_1^{γ} r2(10)
999VW	1005VW[d]	990	990	NC_1^{α} s(26) D_3 r2(20) $C^{\beta}C_2^{\gamma}$ s(13)
	973W[d]	976	976	$C_2^{\alpha}H_2$ r(24) D_3 r2(21)
960VS		963	963	$C_2^{\alpha}H_2$ r(21) N_2D ib(14)
	955W	951	951	$C_3^{\alpha}H_2$ r(48) $C_3^{\alpha}C$ s(24) O_2 ss(10) O_2 b(10)
	934W	928	928	$C_3^{\alpha}H_2$ r(31) N_3D ib(27) $C_3^{\alpha}C$ s(12)
903VW		910	910	N_2D ib(23) C_2N s(12) N_3D ib(7)
900W		905	905	D_3 r1(36) $C^{\beta}C_1^{\gamma}$ s(18) $C^{\beta}C_2^{\gamma}$ s(13)
	877			
834W		836	836	C_1N s(15) D_3 r2(12) D_3 r1(5)
815VW				
801W	800W	806	805	$C^{\beta}C_1^{\gamma}$ s(20) $C^{\beta}C_2^{\gamma}$ s(20) D_3 r1(19) $C_1^{\alpha}C^{\beta}$ s(18)
745W	747W	752	753	O_2 b(36) O_2 ss(11)
736VW	729W	727	727	$C_1^{\alpha}C$ s(13) C_1O ib(10) D_3 r2(9)
	693MW	685	685	C_1O ob(63) C^{β} b1(10)
662MW		650		
	658M		644	C_2O ib(26) $C^{\alpha}CN$ d(12)
595S	596MS	594	594	O_2 w(92)
		570	571	O_2 r(30) $C_2^{\alpha}CN$ d(21)
560MW	558MS	566	566	C_2O ob(61) N_3D ob(10)
510 sh		513	513	C_2N t(63) N_3D ob(29) C_1N t(22) N_2D ob(9)
500S	504VW[d]	501	501	C_1N t(49) N_2D ob(25) C_2N t(18) N_3D ob(5)
			492	C^{γ} b1(13) O_2 r(13) $C_1^{\alpha}CN$ d(11) C_1N t(10)
475W	476S	484		C_1N t(15) C^{γ} b1(12) O_2 r(11) $C_1^{\alpha}CN$ d(10) N_2D ob(6)
439M	442M	450	450	C^{β} d(51)
401MW	401MS	412	414	C^{γ} b2(25) O_2 r(12)
381W	382W	380	381	C^{γ} b2(37) C^{γ} b1(10)

TABLE V

(*Continued from the previous page*)

Observed[a]		Calculated		
Raman	IR	A	B	Potential Energy Distribution[b]
353W	357M	355	354	NC_1^{α} t(42) $D_3 \ldots O$ b(17) $D_3 \ldots O$ s(11) D_3 t(10)
322W	328W	324	324	$NC_2^{\alpha}C$ d(14) C_2O ib(14) N_3D ob(5)
308W			282	C^{γ} b1(18) $NC_1^{\alpha}C$ d(17) $C_1^{\alpha}CN$ d(13)
	286MS	281		$NC_1^{\alpha}C$ d(21) C^{γ} b1(17) $C_1^{\alpha}CN$ d(15)
273MW		263		$NC_3^{\alpha}C$ d(20) O_2 r(11)
	~ 269MS		259	C^{β} b1(13) $NC_3^{\alpha}C$ d(12) $NC_1^{\alpha}C$ d(10)
238M	~ 244MS	254		C^{β} b1(21) C^{γ} b1(13) N_3D ob(6)
			253	CNC_3^{α} d(12) C_2O ib(10) C^{β} b1(10) N_3D ob(6)
	~ 228M	242	240	C^{β} b1(28) CNC_3^{α} d(10) N_3D ob(6)
220 sh	218M	224	223	CNC_2^{α} d(20) CNC_3^{α} d(17) $D_3 \ldots O$ s(7)
	206W 193W	208	208	C^{β} b2(36) $C^{\beta}C_2^{\gamma}$ t(15) N_2D ob(7) $D_3 \ldots O$ s(5)
	185W	198		$C^{\beta}C_1^{\gamma}$ t(67) $C^{\beta}C_2^{\gamma}$ t(25)
			198	$C^{\beta}C_2^{\gamma}$ t(49) $C^{\beta}C_1^{\gamma}$ t(42)
	175W		196	$C^{\beta}C_1^{\gamma}$ t(47) $C^{\beta}C_2^{\gamma}$ t(32)
		195		$C^{\beta}C_2^{\gamma}$ t(54) $C^{\beta}C_1^{\gamma}$ t(33)
162VW	167VW	159	155	$D_3 \ldots O$ s(26) $N_2D \ldots O$ s(6)
144VW	144W	138	138	C^{β} b2(18) $NC_1^{\alpha}C$ d(17) $C_1^{\alpha}CN$ d(13) C_1O ob(11)
	120VW	115		$D_3 \ldots O$ s(18) $N_3D \ldots O$ s(14)
111W	115 sh		107	$D_3 \ldots O$ s(10) $N_2D \ldots O$ s(10) $N_3D \ldots O$ s(10)
			101	$D_3 \ldots O$ s(60) N_2D ob(7)
95W	96W	91		$C_3^{\alpha}C$ t(27) N_2D ob(10) NC_2^{α} t(10) $D_3 \ldots O$ s(7) N_3D ob(6)
			84	$D_3 \ldots O$ s(18) $C_3^{\alpha}C$ t(16) NC_2^{α} t(11) N_2D ob(7)
	87W			$N_2D \ldots O$ s(7) N_3D ob(7)
		82		$N_2D \ldots O$ s(15) $C_1^{\alpha}C^{\beta}$ t(11) $D_3 \ldots O$ s(9)
	76VW		77	$C_3^{\alpha}C$ t(16) $C_1^{\alpha}C^{\beta}$ t(10) $D_3 \ldots O$ s(7) $N_2D \ldots O$ s(6) N_3D ob(5)
70W		69		NC_3^{α} t(22) N_2D ob(13) $C_1^{\alpha}C^{\beta}$ t(13) N_3D ob(10) $N_3D \ldots O$ b(5)
	65 sh		65	NC_3^{α} t(19) N_3D ob(16) $NC_3^{\alpha}C$ d(14) N_3D t(7) $N_3D \ldots O$ b(6)
60VW		61		N_3D ob(19) $NC_3^{\alpha}C$ d(18) $C_1^{\alpha}C^{\beta}$ t(11) $D_3 \ldots O$ s(9)
	54 sh		54	$C_1^{\alpha}C^{\beta}$ t(58) N_3D ob(7) $D_3 \ldots O$ s(6)
	45 VW	49		$C_1^{\alpha}C^{\beta}$ t(48) $D_3 \ldots O$ s(5)
		38		$D_3 \ldots O$ b(17) NC_1^{α} t(14) $D_3 \ldots O$ s(16) $D_3 \ldots O$ t(14) N_2D t(5)
			38	$C_1^{\alpha}C^{\beta}$ t(18) $D_3 \ldots O$ t(11) $NC_2^{\alpha}C$ d(10) NC_3^{α} t(10) N_2D ob(7)
			36	$D_3 \ldots O$ t(17) $D_3 \ldots O$ b(15) $D_3 \ldots O$ s(13)
		33		NC_3^{α} t(18) N_3D t(14) $D_3 \ldots O$ t(13) $N_3D \ldots O$ b(6)
			32	$D_3 \ldots O$ b(14) $C_1^{\alpha}C$ t(11) N_3D t(9) $D_3 \ldots O$ s(8) N_2D t(6)
		29		$D_3 \ldots O$ s(26) $NC_2^{\alpha}C$ d(12) N_2D ob(8)
			23	NC_3^{α} t(18) $D_3 \ldots O$ b(14) $C_2^{\alpha}C$ t(14) NC_1^{α} t(9)
		16		$C_1^{\alpha}C$ t(21) $D_3 \ldots O$ b(14) N_2D t(7) $N_3D \ldots O$ s(6) N_2D ob(6)
			15	$C_1^{\alpha}C$ t(24) N_2D ob(12) $N_3D \ldots O$ s(8) $D_3 \ldots O$ t(6)
		14		$D_3 \ldots O$ b(16) $D_3 \ldots O$ s(12) N_2D ob(10)
		8		$O_2 \ldots D$ b(24) $D_3 \ldots O$ t(23) CO^- t(10)

[a] S, strong; M, medium; W, weak; V, very; sh, shoulder.

[b] s, Stretch; ss, symmetric stretch; as, antisymmetric stretch; b, bend; sb, symmetric bend; ab, antisymmetric bend; ib, in-plane bend; ob, out-of-plane bend; d, deformation; w, wag; tw, twist; r, rock; D_3, ND_3^+; O_2, CO_2^-. Only contributions of 10 or greater are included, except for ND and ND_3^+, for which contributions of 5 or greater are included. In some cases, the value is an average of the PEDs for the A and B species. For the ND_3^+ group, $D_3 \ldots O$ s and $D_3 \ldots O$ b refer to the combined values of the three N-D bonds.

[c] Includes DDC interactions.

[d] Clearly visible in liquid N_2 temperature spectra.

this mode. It is clear that NH_3^+ sb is not as strong in the ir as NH_3^+ ab, and therefore its assignment in VGG is less certain.

The main NH_3^+ rock (r) mode is predicted at 1208 cm^{-1}, and is clearly assigned to the strong Raman band at 1219 cm^{-1} that disappears on N-deuteration. In amino acids, this mode is assigned to bands in the 1220–1238 cm^{-1} region. Contributions from NH_3^+ r are also present in other modes, and their behavior on N-deuteration is consistent with such an assignment: the mainly $C_1^\alpha C^\beta$ s mode at 1316 cm^{-1} is predicted to shift down to 1310 cm^{-1}, and the corresponding observed bands at 1309 (R) and 1307 (ir) cm^{-1} do shift down a few cm^{-1}; the 1267 and 1260 cm^{-1} modes contain NH in-plane bend (ib) as well as NH_3^+ r, so their disappearance is expected in any case, as is observed; the 1136 cm^{-1} mode, mainly NC_2^α s and NC_3^α s, is predicted to shift down to 1129 cm^{-1}, and the distinct shoulder in the Raman at 1135 cm^{-1} disappears and is replaced by a stronger band at 1129 cm^{-1} that undoubtedly also contains the superimposed C^γ r modes previously observed at 1125 (R) and 1129 (ir) cm^{-1}. The ND_3^+ r mode is combined with a number of other modes, but its predicted behavior is well borne out by the observations. One dominant effect is the mixing of ND_3^+ r with the $C^\beta C_1^\gamma$ s and $C^\beta C_2^\gamma$ s of the 835 cm^{-1} mode in VGG to "split" it into two similar modes at 905 and 806 cm^{-1} in VGG-ND; indeed, the strong Raman band at 844 cm^{-1} in the former disappears and is replaced by two new (weak) bands at 900 and 801 cm^{-1} in the latter. This is a good example of how the effects of N-deuteration can be misleading in the absence of the insights provided by normal mode analysis: the disappearance of the 844 cm^{-1} band would otherwise be taken as an indication that this mode contains a significant NH component, leading to its misassignment. In fact, it might be thought that the 844 cm^{-1} band shifts to 834 cm^{-1} in VGG-ND, whereas it can be seen that the latter is an entirely different mode (C_1N s) with a significant ND_3^+ r component. Another effect is the mixing of ND_3^+ r with the $C_2^\alpha H_2$ r mode at 972 cm^{-1}, causing it to "split" into two modes at 976 and 963 cm^{-1} (the latter mixing with N_2D ib); the downshift of the strong 965 cm^{-1} Raman band to 960 cm^{-1} and the appearance of a new ir band at 973 cm^{-1} are consistent with these predictions. The redistribution of $C^\beta C_1^\gamma$ s and $C^\beta C_2^\gamma$ s in the 998 cm^{-1} mode of VGG into modes in VGG-ND at 1003 and 990 cm^{-1}, the latter also containing ND_3^+ r, can account for the disappearance of the 1004 cm^{-1} Raman band and its replacement by bands at 1014 and 999 cm^{-1}. The non-CO_2^- components of the 751-cm^{-1} mode are predicted to combine with ND_3^+ r to give a new mode at 727 cm^{-1}, and the disappearance of a Raman band at 756 cm^{-1} in VGG combined with the appearance of a new ir band at 729 cm^{-1} is consistent with this expectation.

The NH_3^+ torsion (t) mode (designated NC_1^α t in Tables IV and V) is found near 520 cm^{-1} in α-glycine and near 480 cm^{-1} in L-alanine and L-serine. We predict it at 522 and 499 cm^{-1} in VGG, and it is well assigned to a strong Raman band at 515 cm^{-1} that disappears on N-deuteration (a shift to 500 cm^{-1} is counterindicated by the normal mode analysis) and a weak ir band at 506 cm^{-1} that also disappears on N-deuteration. The ND_3^+ t mode is calculated at 355 cm^{-1}, and is assignable to a new Raman band at 353 cm^{-1} and perhaps the medium ir band at 357 cm^{-1} (although overlap with the weak supposed overtone band at 360 cm^{-1} in VGG must be allowed for).

The CO_2^- as mode is generally found in spectra of amino acids at 1590–1595 cm^{-1} (see Table III). We find no definable ir band in this region for VGG, but on N-deuteration, when the strong NH_3^+ ab band is removed, we clearly see a medium-intensity band at 1589 cm^{-1} with a well-defined shoulder (particularly at LN_2 temperature) at 1572 cm^{-1}. These bands are unambiguously assignable to CO_2^- as, which we calculate at 1584 cm^{-1}. The splitting in the observed spectrum probably corresponds to an A-B separation; we do not calculate such a splitting since we have not incorporated a $CO_2^- - CO_2^-$ interaction. However, such an interaction undoubtedly exists, and is probably of the dynamic partial charge type that we have characterized in the formic acid dimer.[25] The CO_2^- ss mode is expected near 1410 cm^{-1} and should clearly be assigned to the strong ir band at 1404 cm^{-1}; we calculate it at 1400 cm^{-1}. We also attribute the Raman band at 1411 cm^{-1} to this mode rather than assigning it to the $C_2^\alpha H_2$ b, $C_2^\alpha H_2$ wag (w) mode calculated at 1416 cm^{-1}, since it does not follow the shift pattern predicted on N-deuteration. The splitting in the CO_2^- ss mode would therefore also be attributed to a coupling between the two molecules in the primitive unit cell.[25]

The assignments of the CO_2^- b, w, and r modes have been controversial, particularly as to whether the highest frequency is a bend or a wag mode. We have followed the order proposed by Destrade et al.,[7] since their assignments were based on spectra of ^{15}N- and ^{18}O-substituted molecules.

Modes with significant contributions from CO_2^- b are calculated at 777 and 751 cm^{-1}, and can be assigned to observed bands near 775 and 757 cm^{-1}, respectively. These assignments are impressively supported by the N-deuteration results: the 777-cm^{-1} CO_2^- b, CO_2^- ss mode is predicted to shift down to 753 cm^{-1} [mainly due to the contribution of a $C_3^\alpha C$ s(9) contribution in the latter case instead of a $C_1^\alpha C$ s(6) contribution in the former], and the observed 775 cm^{-1} band indeed shifts down to 746 cm^{-1}; the 751 cm^{-1} C_1O ib, $C_1^\alpha C$ s mode with a CO_2^- b component is predicted to shift down to 727 cm^{-1} [with CO_2^- b (7) and ND_3^+ r contributions], and indeed the observed 757 cm^{-1} band shifts down to 729 cm^{-1}.

The CO_2^- w mode is predicted to contribute at 595 and 587 cm^{-1} (the latter being mainly CO_2^- r); assignments to observed bands near 593 and 584 cm^{-1} are compelling. On N-deuteration, only the higher frequency mode is expected to remain, and this is indeed what is observed.

The CO_2^- r mode is predicted mainly at 587 cm^{-1}, with a clear assignment to the observed band at 584 cm^{-1}, and it contributes to modes calculated near 418 cm^{-1}, with assignable observed bands at 405 cm^{-1}. On N-deuteration, the former mode is predicted to shift down to 571 cm^{-1}; in fact, the 584 cm^{-1} band disappears and new stronger bands appear near 559 cm^{-1} that, in addition to the C_2O out-of-plane bend (ob) mode near this position, probably contain contributions from the shifted CO_2^- r mode. The 418-cm^{-1} mode is predicted to shift to ~ 413 cm^{-1} on N-deuteration, and the observed bands at 405 cm^{-1} in VGG shift to 401 cm^{-1} in VGG-ND. In addition, CO_2^- r is predicted to contribute, in combination with N_2D ob, to a new mode at 484 cm^{-1} in VGG-ND, and indeed a new band is observed at 475 (R), 476 (ir) cm^{-1}.

We see, therefore, that the modes of the NH_3^+ and CO_2^- end groups are very well accounted for by the normal mode analysis. This is the case even though

some of the frequencies, although not the force constants, differ significantly (particularly for the CO_2^- b, w, and r modes) from those of the amino acids (cf. α-glycine[7] in Table III).

AMIDE MODES

The amide I, II, III, and V modes are found to be particularly sensitive to chain conformation,[1] and it is therefore important to see how well they are reproduced by the calculation. As in other polypeptide systems,[1] electrostatic coupling between similar amide I and amide II modes in the unit cell leads to significant frequency shifts. We calculate these interactions, as noted above, in the DDC formalism[9] rather than the TDC formalism used previously.[1] For the amide I, II, and V modes, we have also calculated the $|\partial\mu/\partial Q|^2$, to which the ir intensities are proportional.

The normal mode calculation predicts amide I frequencies for VGG at 1669 (A), 1663 (A), 1669 (B), and 1663 (B) cm^{-1}. When DDC is incorporated, these shift to (with relative $|\partial\mu/\partial Q|^2$ in parentheses) 1643 (5.4), 1645 (9.4), 1654 (1.5), and 1661 (1.7) cm^{-1}, respectively. The very strong ir band observed at 1645 cm^{-1} is clearly assignable to the first two modes, whereas the weak ir band at 1663 cm^{-1} can be assigned to the 1661 cm^{-1} mode. We assign the very strong Raman band at 1657 cm^{-1} to the calculated 1654 cm^{-1} mode, since we feel, in the light of average ir/Raman coincidences in the spectrum, it is not at the same frequency as the 1663 cm^{-1} ir band. Thus, the amide I modes of VGG are excellently reproduced by our calculations.

As expected,[1] there is a small downshift in the amide I frequencies on N-deuteration. For VGG-ND, we calculate unperturbed frequencies at 1665 (A), 1659 (A), 1665 (B), and 1659 (B) cm^{-1}. When DDC is incorporated, these frequencies (and their relative $|\partial\mu/\partial Q|^2$) are predicted at 1639 (5.4), 1641 (9.6), 1650 (1.7), and 1657 (1.8) cm^{-1}, respectively. The first two modes clearly are associated with the very strong ir band at 1640 cm^{-1}; the downshift from VGG is very well predicted. The second two modes correlate well with observed bands at 1650VS (R) and 1661W (ir) cm^{-1}, respectively, again reflecting the shifts associated with N-deuteration.

The unperturbed amide II modes of VGG are predicted at 1548 (A), 1538 (A), 1548 (B), and 1538 (B) cm^{-1}. When DDC is included, the shifted frequencies (and their $|\partial\mu/\partial Q|^2$) become 1595 (0.7), 1531 (0.0), 1564 (0.5), and 1541 (12.4) cm^{-1}, respectively. The strong ir band at 1543 cm^{-1} and the medium-weak Raman band at 1541 cm^{-1}, both of which disappear on N-deuteration, are clearly assignable to the 1541 cm^{-1} mode. The very weak shoulder at 1568 cm^{-1} in the ir is most likely assignable to the predicted very weak band at 1564 cm^{-1}. No comparable band is seen, as might be expected, near 1595 cm^{-1}, but this could be a result of overlap with the CO_2^- as mode, observed more easily in VGG-ND, at 1589 cm^{-1}. Otherwise, the observed bands are in excellent agreement with the predicted frequencies, as is the general amide II/amide I intensity ratio. It is also interesting to note that, whereas the ir-strong unperturbed frequency at 1535 cm^{-1} in poly(glycine) I[1] shifts down with TDC interactions to 1515 cm^{-1} and is observed very near this value, in VGG the unperturbed mode at 1538 cm^{-1} (also associated with glycine residues) is shifted to 1541 cm^{-1} after DDC interactions and is

observed near this value. These differences are a result of the different interactions in the two different structures, and the excellent predictions in both cases testify to the validity of the interaction mechanisms we have proposed.[1,25]

On N-deuteration, the so-called amide II′ modes are calculated at 1490 and 1481 cm^{-1}, and new bands are seen at 1491 and 1480 cm^{-1}. The resulting ND ib is predicted to contribute to modes at 1040, 1034, 1033, 963, 928, and 910 cm^{-1}. Assignments to these modes are indicated in Table V; although satisfactory, they may be somewhat uncertain because of the weakness of most of the bands. However, the predicted downward shift of the 972 cm^{-1} $C_2^{\alpha}H_2$ r mode to 963 cm^{-1} as a result of mixing with N_2D ib is mirrored by the downward shift of the strong Raman band at 965 to 960 cm^{-1}, confirming both assignments.

The NH ib coordinate also contributes to modes in the ~ 1400–1200-cm^{-1} region that, when combined with CN s, have been referred to as amide III, although the CN s contribution is not necessarily always present.[1] In VGG such modes are predicted (including DDC interactions) at 1389, 1267, 1260, and 1238 cm^{-1} (the unperturbed frequencies are 1389, 1274, 1263, and 1238 cm^{-1}), and their assignment is substantiated by their behavior on N-deuteration. (We are not able at present to provide calculated ir intensities for these modes, since the $\partial\mu/\partial S$ for eigenvector components such as H^{α} b, H^{β} b, NH_3^+ r, CH_2 w, and CH_2 tw are not presently available.[20]) The medium-weak Raman band at 1379 cm^{-1}, assignable to the first mode, is replaced in VGG-ND by a weak band at 1373 cm^{-1}, a result of $C^{\gamma}H_2$ sb mixing with $C_3^{\alpha}H_2$ w to produce two new modes calculated at 1368 and 1366 cm^{-1}. The other three modes, observed at 1264 (R), 1259 (ir), and 1235 (R, ir) cm^{-1}, are all replaced on N-deuteration by different eigenvectors in this region, in good agreement with observation: H^{β} b1 is predicted to shift from 1267 to ~ 1226 cm^{-1}, which can account for the residual band remaining at 1235 cm^{-1}; $C_3^{\alpha}H_2$ w is now completely concentrated in the 1368, 1366 cm^{-1} modes; and the $C_2^{\alpha}H_2$ tw and $C_3^{\alpha}H_2$ tw contributions to the 1238 cm^{-1} mode (as well as to unobserved modes at 1251 and 1242 cm^{-1}) are now concentrated in two modes at 1277 and 1246 cm^{-1}, corresponding to new bands at 1280 (R), 1282 (ir) and 1250 (R, ir) cm^{-1}. Again, we see the complexity of the changes that occur on N-deuteration and how well they are accounted for by our force field.

The amide V modes combine NH ob with CN t, and are usually strong in the ir and weak in the Raman. They are, of course, expected to be affected by N-deuteration, and this is true of the five such modes that we calculate at 698, 677, 662, 654, and 566 cm^{-1} (including DDC contributions of 0, +5, 0, +3, and +2 cm^{-1}) and their assigned ir bands at 714, 675, 670, 647, and 564 cm^{-1}, respectively. [The calculated $|\partial\mu/\partial Q|^2$ of these modes are 2.8, 0.3, 0.4, 2.5, and 1.2, respectively. Observed ir bands corresponding to the latter three modes have relative intensities in reasonable agreement with those calculated. This is not true for the first two modes, which are the ones containing contributions from CN t. This may be due to the large uncertainty in the $(\partial\mu/\partial S)$ for CN t.[9]] The 698 and 677 cm^{-1} modes are essentially pure amide V, and they "disappear" on N-deuteration. The 662 and 654 cm^{-1} modes are mostly C_1O ob, which is predicted to shift completely up to 685 cm^{-1} in VGG-ND; indeed, a new band is observed at 693 cm^{-1}. The C_2O ib component

of the 654 cm^{-1} mode is predicted to shift to 650 (A), 644 (B) cm^{-1} in VGG-ND, and, although the observed shift is in the opposite direction, this appears to be a reasonable explanation for the 658 cm^{-1} band remaining after N-deuteration. The 566 cm^{-1} mode is mainly C_2O ob, which is predicted to remain at 566 cm^{-1} in VGG-ND, where it is mixed with N_3D ob and probably overlapped by the shifted CO_2^- r mode; the new strong band appearing at 558 cm^{-1} is consistent with these assignments. The ND ob coordinate, in addition to contributing at 566 cm^{-1} and to a new mode at 513 cm^{-1}, for which a shoulder is observed in the Raman, is predicted to contribute to new modes at 501 and 484 cm^{-1}, and strong new bands are observed at 500 (R) and 476 (ir) cm^{-1} in VGG-ND that can be assigned to these modes. The apparent "shift" of the strong 515 cm^{-1} Raman band of VGG to 500 cm^{-1} is therefore accounted for naturally by the calculation. Thus, the amide V bands are well predicted by the calculations, as are other bands in this spectral region.

OTHER MODES

We comment here on the assignment of some other bands in the spectra, based on the normal mode calculations.

The assignments of the CH_2 and CH_3 stretch modes are complicated by the overlapping bands and the presence of Fermi resonances in this region.[26] Nevertheless, many assignments are relatively straightforward. The observed bands at 2972S (R) and near 2968M (ir) cm^{-1} are clearly assignable to CH_3 as, while the band at 2945VW (ir) cm^{-1} may be due to CH_3 ss.[27] The $C_3^\alpha H_2$ as mode is located above 3000 cm^{-1} in triglycine (T. Sundius, J. Bandekar, & S. Krimm, to be published) and a similar assignment is indicated in VGG; the $C_3^\alpha H_2$ ss mode is then reasonably assigned to the 2930VW (R, ir) cm^{-1} bands. The $C_2^\alpha H_2$ as and $C_2^\alpha H_2$ ss modes are satisfactorily assigned to bands at 2926 sh(ir) an 2850 sh(R, ir) cm^{-1}, respectively. The frequencies of CH s modes are sensitive to the C—H bond length, and its force constant, in its dependence on local structure.[27] Values of 2902 and 2870 cm^{-1} for these modes are reasonable,[27] and the assignments given in Table IV follow. A band near 2875 cm^{-1} has been found to be in Fermi resonance with the CH_3 ss mode near 2940 cm^{-1},[27] and is so assigned here. We have no clear assignment of the 2992 sh(R) cm^{-1} band (unless it is part of the group of CH_3 as modes).

The assignments of all the CH_2 b and CH_3 ab modes made in Tables IV and V cannot be specific at the present time, although the observed bands in the ~ 1470–1450-cm^{-1} region are basically accounted for. We have already noted that CH_3 sb is concentrated in two modes, at 1366 and 1363 cm^{-1}, in VGG but is distributed over four modes, at 1368, 1366, 1364, and 1362 cm^{-1}, in VGG-ND, and this seems to be in good accord with observation.

A number of modes in the midfrequency range retain their character on N-deuteration but are predicted to shift in frequency, and these shifts are well reproduced by the calculations. Thus, the H^α b1 mode at 1168 cm^{-1} is predicted to shift to 1188 cm^{-1}, and the observed 1171 cm^{-1} band of VGG indeed shifts to 1187 (ir) cm^{-1} in VGG-ND; the NC_1^α s mode at 1013 cm^{-1} is predicted to shift up slightly, to 1017 cm^{-1}, and the very strong Raman band at 1027 cm^{-1} shifts to 1029 cm^{-1}; and the complex mode at 998 cm^{-1} is predicted to shift to 1003 cm^{-1}, with the observed bands shifting from 1004 to 1014 cm^{-1}.

In the low-frequency region, shifts of similar modes on N-deuteration are also predicted and observed. As in the case of the amide V modes, the observed shifts are not always in the same direction as those predicted. However, in view of the expected accuracy of the force field, the general agreement is quite acceptable. Such shifts, with assigned observed bands in parentheses, include 445 (444) to 450 (441), 418 (405) to 413 (401), 394 (385) to 381 (381), 327 (325) to 324 (325), 298 (311) to 281 (288), 295 (297) to 282 (308), 271 (280) to 263 (273), 267 (277) to 259 (269), and 262 (260) to 254 (241) cm^{-1}. Analogous comparisons can be made for lower frequency modes, but their assignments must be considered tentative at this stage, particularly since nonbonded interactions, which would be expected to influence lattice and similar low-lying modes, have not been incorporated into our calculations. The specific features of the other assignments, however, lend confidence to the general validity of our normal mode calculations.

CONCLUSIONS

We have analyzed the ir and Raman spectra of VGG and VGG-ND from the point of view of testing our polypeptide force fields[1] for their ability to explain the spectra of a known parallel-chain β-structure, one that was not included in the original refinement process. We find that the predicted normal mode frequencies, including those of end groups, are in very good agreement with the observed bands: the average discrepancy between observed and calculated frequencies below 1700 cm^{-1} is 5.1 cm^{-1}. In particular, subtle as well as major changes in normal modes that are predicted to occur on N-deuteration are in fact found in the observed spectra of VGG-ND, including changes in modes that do not contain contributions from NH coordinates. These changes are undoubtedly specific to this structure, and serve as an important measure of the validity of our force fields. This kind of detailed evaluation of the normal mode origin of observed spectral bands and of their changes on isotopic substitution is necessary in order to be assured that the analysis is reliable.

In addition to calculating normal mode frequencies, we have also computed ir intensities of amide I, II, and V modes, using dipole derivatives obtained from ab initio calculations on the peptide group.[9] The agreement with observed band intensities is very good for the amide I, amide II, and three of the five modes containing NH ob. For the other two amide V modes, uncertainty in the dipole derivative for CN t^9 makes it difficult to evaluate the discrepancies at this time. It is nevertheless clear that calculated intensities can provide important independent information on polypeptide conformation.

The satisfactory analysis of the vibrational spectra of VGG provides the basis for confidence in the predictions for the parallel-chain β-sheet structure.[5]

This research was supported by NSF grants DMB-8517812 and DMR-8303610.

References

1. Krimm, S. & Bandekar, J. (1986) *Adv. Protein Chem.* **38**, 181–364.
2. Sengupta, P. K. & Krimm, S. (1987) *Biopolymers* **26**, S99–S107.
3. Richardson, J. S. (1981) *Adv. Protein Chem.* **34**, 167–339.

4. Toniolo, C. & Palumbo, M. (1977) *Biopolymers* **16**, 219–224.
5. Bandekar, J. & Krimm, S. (1988) *Biopolymers* **27**, 909–921.
6. Lalitha, V., Murali, R. & Subramanian, E. (1986) *Int. J. Peptide Protein Res.* **27**, 472–477.
7. Destrade, C., Garrigou-Lagrange, C. & Forel, M.-T. (1971) *J. Mol. Struct.* **10**, 203–219.
8. Cheam, T. C. & Krimm, S. (1984) *Chem. Phys. Lett.* **107**, 613–616.
9. Cheam, T. C. & Krimm, S. (1985) *J. Chem. Phys.* **82**, 1631–1641.
10. Turrell, G. (1972) *Infrared and Raman Spectra of Crystals*, Academic Press, New York.
11. Dwivedi, A. M. & Krimm, S. (1982) *Macromolecules* **15**, 177–185.
12. Dwivedi, A. M. & Krimm, S. (1982) *Macromolecules* **15**, 186–193.
13. Dwivedi, A. M. & Krimm, S. (1983) *Macromolecules* **16**, 340.
14. Snyder, R. G. & Schachtschneider, J. H. (1965) *Spectrochim. Acta* **21**, 169–195.
15. Krimm, S. & Abe, Y. (1972) *Proc. Natl. Acad. Sci. USA* **69**, 2788–2792.
16. Moore, W. H. & Krimm, S. (1975) *Proc. Natl. Acad. Sci. USA* **72**, 4933–4935.
17. Machida, K., Kagayama, A., Saito, Y., Kuroda, Y. & Uno, T. (1977) *Spectrochim. Acta* **33A**, 569–574.
18. Wang, C. H. & Storms, R. D. (1971) *J. Chem. Phys.* **55**, 3291–3299.
19. Adamowicz, R. F. & Sage, M. L. (1974) *Spectrochim. Acta* **30A**, 1007–1019.
20. Machida, K., Kagayama, A., Saito, Y. & Uno, T. (1978) *Spectrochim. Acta* **34A**, 909–914.
21. Susi, H. & Byler, D. M. (1980) *J. Mol. Struct.* **63**, 1–11.
22. Diem, M., Polavarapu, P. L., Oboodi, M. & Nafie, L. A. (1982) *J. Am. Chem. Soc.* **104**, 3329–3336.
23. Susi, H., Byler, D. M. & Gerasimowicz, W. V. (1983) *J. Mol. Struct.* **102**, 63–79.
24. Krimm, S. & Dwivedi, A. M. (1982) *J. Raman Spectrosc.* **12**, 133–137.
25. Dybal, J., Cheam, T. C. & Krimm, S. (1987) *J. Mol. Struct.*, **159**, 183–194.
26. Snyder, R. H., Hsu, S. L. & Krimm, S. (1978) *Spectrochim. Acta* **34A**, 395–406.
27. Cheam, T. C. & Krimm, S. (1987) *Spectrochim. Acta*, in press.

Received July 8, 1987
Accepted December 10, 1987